RESEARCH ARTICLE | SEPTEMBER 24 2024

The steady-state solution of wave–current interaction based on the third-order Stokes wave theory

Ming Ni (倪明) ; Kai Wei (魏凯) ; Min Luo (罗敏) ; Jinghua Wang (王菁华)

Physics of Fluids 36, 097153 (2024)
https://doi.org/10.1063/5.0219237

Physics of Fluids ARTICLE pubs.aip.org/aip/pof

The steady-state solution of wave–current interaction based on the third-order Stokes wave theory

Cite as: Phys. Fluids **36**, 097153 (2024); doi: 10.1063/5.0219237
Submitted: 16 May 2024 · Accepted: 5 September 2024 ·
Published Online: 24 September 2024

Ming Ni (倪明),[1] Kai Wei (魏凯),[1,a)] Min Luo (罗敏),[2] and Jinghua Wang (王菁华)[3]

AFFILIATIONS

[1]State Key Laboratory of Bridge Intelligent and Green Construction, Southwest Jiaotong University, Chengdu 610031, China
[2]Ocean College, Zhejiang University, Zhoushan, Zhejiang 316021, China
[3]Department of Civil and Environmental Engineering, The Hong Kong Polytechnic University, Hong Kong 999077, China

[a)]Author to whom correspondence should be addressed: kaiwei@home.swjtu.edu.cn

ABSTRACT

This manuscript reports on the interaction of a current-free monochromatic surface wave field with a wave-free uniform current field. The existing reasonable theories of wave–current interactions are primarily based on weak current assumptions and derived from linear theory, resulting in calculation bias in the analysis of nonlinear wave–current interactions. Moreover, experimental data on high-order wave–current interactions still need to be collected. Thus, steady-state solutions named the third-order wave–current theory based on the third-order wave dispersion relationship and the principle of wave–current energy conservation were derived. The wave–current interaction experiment was set up to cover 164 sets of experimental conditions, including 33 types of periodic waves from the second to the fifth order and six different current velocities. The effects of water depth, current velocity, wave period, and height on the wave height and wavelength in the wave–current interaction field were investigated. A comparison of the mean relative error (MRE) and the determination coefficient (R^2) of the wavelength with the experimental data revealed that the third-order wave–current theory outperformed the traditional linear theory, with an optimal reduction of 75% and an enhancement of 25%, respectively. Additionally, the third-order wave–current theory reduces the MRE by 25%–40% in the wave height calculation, with R^2 consistently outperforming the linear theory. The third-order wave–current theory can significantly improve the calculation accuracy of the theoretical method in solving nonlinear wave–current interactions.

NOMENCLATURE

a	Wave amplitude after the interaction
a'	Short-wave amplitude
a_1	Wave amplitude after the interaction
a_2	Wave amplitude of long waves
a_s	Wave amplitude of the current-free wave field
C_g	Wave energy transfer velocity after the interaction
C_{gs}	Wave energy transfer velocity of the current-free wave field
d	Water depth from the still water surface to the bottom
E	Total energy under the free surface after the interaction
E_s	Total energy under the free surface of the current-free wave field
g	Gravitational acceleration
H	Wave height after the interaction
H_1	Wave height calculated by linear theory under the selected conditions
H_{Exp}	Actual wave height data obtained from the wave gauge in the experiment
H_s	Wave height of the current-free wave field
H_T	Wave height calculated by third-order wave–current theory
k_2	Wavenumber of long waves
L	Wavelength after the interaction
L'	Short wavelength
L_1	Wavelength calculated by linear theory for the selected conditions
L_{Exp}	Actual wavelength data collected from experiments
L_s	Wavelength of current-free wave field
L_T	Wavelength calculated by third-order wave–current theory

MWL	Mean water level
SWL	Still water level
U	Current speed
u_x	Horizontal velocities of wave particles
u_z	Vertical velocity of wave particles
x	Horizontal directions
z	Vertical directions
ε	Dimensionless constant independent of the wave characteristic values
η	Wave surface equation at the free water surface
$\eta(x, t)$	Wave surface equation for linear theory
$\eta'(x, t)$	Wave surface equation for third-order waves
ρ	Water density
ϕ	Velocity potential function
ω_r	Relative angular frequency
ω_s	Angular frequency of the combined wave–current field

I. INTRODUCTION

In most of the ocean waters, waves and currents are always experienced at the same time. The waves are usually generated by wind, while the currents can be generated by, for example, waves, density variations, tides, etc. The interaction between waves and currents is vital to structural and operational safety of coastal and offshore infrastructures, including sea-crossing bridges, offshore platforms, and offshore wind turbine.[1] Cattrell *et al.*[2] conducted a study spanning from 2007 to 2015 on 102 collapsed bridges in United States and Australia, and revealed that 43.1% of bridge collapses were attributed to hydrological disasters. Among these factors, the action of waves and currents has been identified as two critical factors causing bridge damages and failures.[3] Waves are influenced by currents, leading to variations in wave height, wavelength, and other characteristics,[4] which requires an enhanced understanding of offshore structures and coastal hazard mitigation.[5]

Many experimental studies have been carried out to study the interaction between waves and current. The interaction experiments between linear regular waves and current showed that a following current results in decreased wave height and increased wavelength, while the opposing current results in the adverse phenomenon.[6] Lodahl *et al.*[7] indicated that the ratio of the current speed over the wave celerity plays a crucial role in the interaction between waves and currents. Such phenomenon is related to the Doppler shift theory, and theoretical investigations have been made by many researchers using the dispersion relation under the steady-state assumption.[8–10] Unna[11] investigated the effect of currents on wave propagation and propose a steady-state solution of waves based on the variation in wave steepness under the influence of tidal currents. Longuet-Higgins and Stewart[12] developed a new steady-state solution on the basis of Unna's theory considering the effect of radiation stress on the wave–current interactions. Zaman and Baddour[13] investigated the amplitude changes of waves propagating in currents and proposed a wave–current coupling steady-state solution based on mass, momentum, and energy conservation equations. Li[14] derived the steady-state solution to calculate changes in wave parameters within a specific range and evaluate errors. Zou[15] provided the steady-state solution to obtain the velocity and pressure distributions under wave–current interaction conditions. The commonly used steady-state solutions are summarized in Table I.

Despite the success of those theories for simulating the interactions between wave and current, Chen *et al.*[16] conducted experiments on the particle trajectories of third-order waves in the presence of the following and opposing currents and stated that the steady-state assumption is not always acceptable for the nonlinear wave and current interaction. Many scholars have conducted some research on the nonlinear wave motions in the presence of steady uniform currents,[17,18] and Baddour and Song[19] developed the first- and second-order water waves on shear currents together with their corresponding dispersion relations and flow characteristics. Craik and Leibovich[20] derived the governing equations for weak currents in the presence of

TABLE I. Summary of the steady-state solutions obtained via wave–current interaction analysis.

Research subject	Steady-state solution	Reference
L, a	$\frac{L'}{L} = 1 - a_2 k_2 \coth k_2 d, \quad \frac{a'}{a_1} = 1 + a_2 k_2 \coth k_2 d$	Unna[11]
a	$\frac{a'}{a_1} = 1 + a_2 k_2 \left(\frac{3}{4}\coth k_2 d + \frac{1}{4}\tanh k_2 d\right)$	Longuet-Higgins *et al.*[12]
L, H	$\frac{L}{L_s} = \left(1 + \frac{U}{C_s}\Big/\frac{L}{L_s}\right)^{-2}\frac{\tanh kd}{\tanh k_s d}$ $\frac{H}{H_s} = \left(1 - \frac{U}{C_s}\Big/\frac{L}{L_s}\right)^{\frac{1}{2}}\left(\frac{L_s}{L}\right)^{\frac{1}{2}}\left(\frac{C_{gs}}{C_g}\right)^{\frac{1}{2}}\left(1 + \frac{U}{C_s}\frac{2 - C_g}{C_g}\Big/\frac{L}{L_s}\right)^{-\frac{1}{2}}$	Li[14]
L, H	$\frac{L}{L_s} = \frac{\tanh kd}{4\tanh k_s d}\left(1 + \left(1 + 4\frac{U}{C_s}\frac{\tanh k_s d}{\tanh kd}\right)^{1/2}\right)^2$ $\frac{H}{H_s} = \left[\frac{k\left(c_{gs}/c_{r0} + U_s/c_{rs}\right)}{k_0\left(c_g/c_r + U/c_r\right)}\right]^{1/2}$	Zou[15]
L	$\frac{L^2}{L_s} = \frac{U}{C_s} + \frac{L}{L_s}\left(\tanh\left(kd\frac{L_s}{L}\right)\coth(k_s d_s)\right)^{1/2}$	Zaman[13]

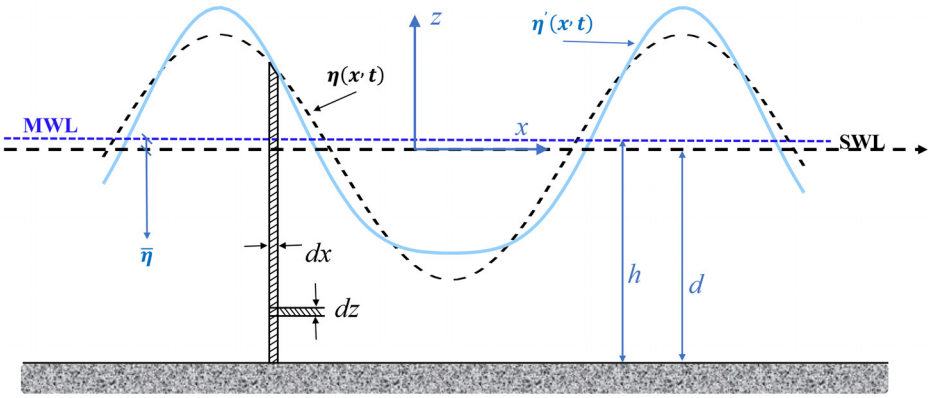

FIG. 1. Sketch of different free surfaces.

high-order surface waves under the assumptions of discrete irrotational gravity waves and homogeneous and of infinite water depth. Zaman *et al.*[21] developed a second-order numerical model based on depth averaged equations and a relevant physical model for the deformation of the water wave propagating over a submerged parabolic obstacle in the presence of uniform current. Hsu *et al.*[22] presented a new third-order trajectory solution in Lagrangian form for the water particles in a wave–current interaction flow based on a Euler–Lagrange transformation. Constantin *et al.*[23] provided second- and third-order approximations to periodic traveling wave profiles and to the velocity field and the pressure beneath the waves, in flows with constant vorticity over a flat bed. Liao *et al.*[24] derived a new theoretical formula to predict the maximum amplitude of waves under following and opposing currents considering the second-order wave group velocity. With the development of computation technology, many numerical models were developed to elucidate the effects of nonlinear wave–current interactions. Wang *et al.*[25] proposed new equations that describe the three-dimensional, fully nonlinear interaction between waves and horizontal shear ocean currents. Zhao *et al.*[26] developed an effective wave–current generation and absorption numerical wave tank, which can simulation linear, nonlinear, and transitional wave–current interactions. All above works show that the high-order harmonic wave components are more sensitive to the current speed than the first-order component.

Although considerable research progress has been made regarding nonlinear wave–current interaction, few closed-form solutions have been developed to express the high-order waves in the presence of following and opposing current. This paper derives the solution of third-order wave–current interaction on the basis of the third-order wave dispersion relationship and the principle of wave–current energy conservation. 164 experimental cases were then conducted to supplement the research database of nonlinear waves in the presence of the following current. The effects of water depth and current velocity on crucial factors such as wave height, wave celerity, and wavelength in the wave–current interaction field were measured and compared to verify the developed solution.

II. MATHEMATICAL FORMULATION

In linear theory, the free liquid surface of third-order waves is described by a sharper crest and flatter trough than small amplitude waves. This study does not explicitly consider the influence of this liquid surface elevation, and the still water height is chosen to correspond to d rather than h, as shown in Fig. 1. The mean water level is set at the origin of the coordinates, and the mean is equal to zero.

A. Governing equations

The wave–current field formula is derived based on the assumption of irrotational and inviscid currents. When the waves encounter uniform and steady water currents, they interact, giving rise to what is known as the wave–current field. The wave–current interaction is assumed to be a stable, uniform, and irrotational combined wave–current field.[27] The potential function satisfies the Laplace equation within the domain, as shown in Eq. (1):

$$\frac{\partial^2\phi}{\partial x^2}+\frac{\partial^2\phi}{\partial z^2}=0, \quad \text{in} \quad -\infty<x<\infty, -d<z<\eta(x,t). \tag{1}$$

For solid boundaries, the impermeability and slip conditions must be satisfied, i.e., at $z=-d$, the seabed conditions are satisfied, as shown in the following equation:

$$\frac{\partial\phi}{\partial z}=0, \quad \text{on } z=-d. \tag{2}$$

The integrated kinematic and dynamic free surface boundary conditions on a free surface, $z=\eta$, can be expressed as shown in the following equation:

$$\frac{\partial^2\phi}{\partial t^2}+g\frac{\partial\phi}{\partial z}+\left[\frac{\partial}{\partial t}+\frac{1}{2}\left(\frac{\partial\phi}{\partial x}\frac{\partial}{\partial x}+\frac{\partial\phi}{\partial z}\frac{\partial}{\partial z}\right)\right]\left[\left(\frac{\partial\phi}{\partial x}\right)^2+\left(\frac{\partial\phi}{\partial z}\right)^2\right]=0, \quad \text{at } z=\eta. \tag{3}$$

By substituting the free surface boundary conditions and the bottom boundary conditions into the water wave governing equations and solving the equations by the perturbation expansion method up to the third order,[28] the free surface wave equation and the velocity potential can be obtained as shown in the following equation:

$$\begin{aligned}\phi&=\sum_{n=1}^{\infty}\epsilon^{n-1}\phi_n=\phi_1+\epsilon\phi_2+\epsilon^2\phi_3\ldots,\\ \eta&=\sum_{n=1}^{\infty}\epsilon^{n-1}\eta_n=\eta_1+\epsilon\eta_2+\epsilon^2\eta_3\ldots,\end{aligned} \tag{4}$$

where ε is dimensionless constant independent of the wave steepness.

B. Third-order wave–current interaction theory

The spatial derivative of the velocity potential ϕ can be used to obtain the horizontal (u_x) and vertical (u_z) velocities of wave particles, as shown in the following equation:

$$\begin{aligned} ux &= \frac{\partial \phi}{\partial x}, \\ uz &= \frac{\partial \phi}{\partial z}. \end{aligned} \tag{5}$$

The measurement of potential energy must be relative to a horizontal plane. The phase-averaged potential energy E_p and kinetic energy E_k over a wavelength are given as follows, and the total energy E_s under the free surface of the current-free wave field is developed as follows in the following equation:

$$\begin{aligned} E_p &= \int_x^{x+L} \int_0^{\eta} \rho g z \mathrm{d}z \mathrm{d}x, \\ E_k &= \int_x^{x+L} \int_{-d}^{\eta} \frac{1}{2} \rho \left(u_x^2 + u_z^2\right) \mathrm{d}z \mathrm{d}x, \\ E_s &= E_p + E_k. \end{aligned} \tag{6}$$

The relative angular frequency ω_r and wavenumber k for progressive waves are determined by the Doppler equation, as shown in the following equation:

$$\begin{aligned} \omega_{\mathrm{r}} &= \sqrt{gk \tanh kd}, \\ \omega_s &= \omega_{\mathrm{r}} + kU. \end{aligned} \tag{7}$$

When using linear theory, the wave energy transfer velocity C_{gs} of the current-free wave field can be calculated by the following equation:

$$\begin{aligned} \mathrm{C}_{gs} &= \frac{C_s}{2}\left(1 + \frac{2 \sinh kd}{\sinh 2kd}\right), \\ \mathrm{C}_g &= \frac{C}{2}\left(1 + \frac{2 \sinh kd}{\sinh 2kd}\right), \end{aligned} \tag{8}$$

where C_g and C are wave energy transfer velocity and wave celerity after the wave–current interaction, respectively, and C_s is wave celerity of the current-free wave field.

According to Longuet-Higgins and Stewart,[12] the conservation equation of the wave action can be written as follows:

$$\frac{\partial}{\partial x}[E(c_{\mathrm{g}} + U)] + S_{xx}\frac{\partial U}{\partial x} = 0, \tag{9}$$

where E is the total energy under the free surface after the wave–current interaction and S_{xx} is radiation stress.

Christoffersen[29] noted that the current gradient term $\partial U/\partial x$ is ignored when considering wave propagation in steady and uniform currents. Thus, the wave–current energy conservation equation can be simplified as shown in the following equation:

$$\frac{d}{dx}\left[\frac{E}{\omega_{\mathrm{r}}}(c_{\mathrm{gs}} + U)\right] = 0. \tag{10}$$

Combining Eqs. (7) and Eq. (8), Eq. (10) can be rewritten as Eq. (11), in the equation E and E_s can be obtained from the formula $E = \rho g H^2/8$ and $E_s = \rho g H_s^2/8$ when they are linear waves.

$$\frac{E}{E_s} = \left(1 - \frac{U}{C_s}\right)\left(\frac{L_s}{L}\right)\left(\frac{C_{gs}C}{C_g C_s}\right)\left(1 + \frac{U}{C_s}\frac{2C - C_g}{C_g} \Big/ \frac{L}{L_s}\right)^{-1}, \tag{11}$$

where E and E_s can be obtained from the formulas $E = \rho g H^2/8$ and $E_s = \rho g H_s^2/8$ for linear waves and H and H_s are the wave heights of the current-free wave field and wave–current field, respectively.

The wave height expressions for a first-order variation are the same as those of Li,[14] but are expressed in different forms as shown in the following equation:

$$\frac{H}{H_s} = \left(1 - \frac{U}{C_s} \Big/ \frac{L}{L_s}\right)^{\frac{1}{2}}\left(\frac{L_s}{L}\right)^{\frac{1}{2}}\left(\frac{C_{gs}C}{C_g C_s}\right)^{\frac{1}{2}}\left(1 + \frac{U}{C_s}\frac{2C - C_g}{C_g} \Big/ \frac{L}{L_s}\right)^{-\frac{1}{2}} = R. \tag{12}$$

Notably, the focus of this paper is on the wavelength variation under the following current, and the dispersion relation for third-order waves[28] is given by the following equation:

$$L = \frac{gT^2}{2\pi}\tanh kd\left[1 + \left(\frac{2\pi a}{L}\right)^2 \frac{14 + 4\cosh^2 2kd}{16 \sinh^4 kd}\right]. \tag{13}$$

Under steady and uniform current conditions, the period of waves remains unchanged after interaction with the current, thus $T = T_s$, as shown in the following equation:

$$\frac{L}{T} = U + \frac{L_s}{T_s}, \tag{14}$$

where L and L_s are the wavelengths of the current-free wave field and the wave–current field, respectively.

Equations (13) and (14) can be combined to derive the formula for the wavelength of the steady-state field after nonlinear wave–current interactions, as shown in the following equation:

$$\begin{aligned} \frac{L}{L_s} &= \left(\frac{L}{L_s} - \frac{U}{C_s}\right)^{-1}\sqrt{\frac{L}{L_s}\left(\frac{M}{M_s}\right)}, \\ M &= \tanh kd \frac{16L^2 + (2\pi a)^2(14 + 4\cosh^2 2kd)}{\sinh^4 kd}, \\ M_s &= \tanh k_s d \frac{16L^2 + (2\pi a_s)^2(14 + 4\cosh^2 2k_s d)}{\sinh^4 k_s d}, \end{aligned} \tag{15}$$

where the equations M and M_s are set nonlinear coefficients of current-free wave field and wave–current field, respectively, which can reflect the nonlinear effect more accurately in wave–current interaction.

The wave energy equation of a third-order wave can be obtained from the following equation:

$$\begin{aligned} E_s &= \frac{\pi a^3}{L}\left\{1 + \pi^2\left(\frac{2\mathrm{a}_s}{L_s}\right)^2\left[B_s + \frac{3}{8192}\pi^2\left(\frac{2\mathrm{a}_s}{L_s}\right)F_s\right]\right\}, \\ B_s &= \frac{1}{2}\left(\frac{1}{\tanh k_s d}\right)^2\left(1 + \frac{3}{1 + 2(\sinh k_s d)^2}\right)^2 + \frac{9}{32}\frac{\cosh 2k_s d}{(\sinh k_s d)^6}, \\ F_s &= 3\left(\frac{1 + 8(\cosh k_s d)^8}{(\sinh k_s d)^6}\right)^2 + \frac{1}{2}\frac{\tanh k_s d \sinh 6k_s d(11 - 2\cosh 2k_s d)^2}{(\sinh k_s d)^{14}}, \end{aligned} \tag{16}$$

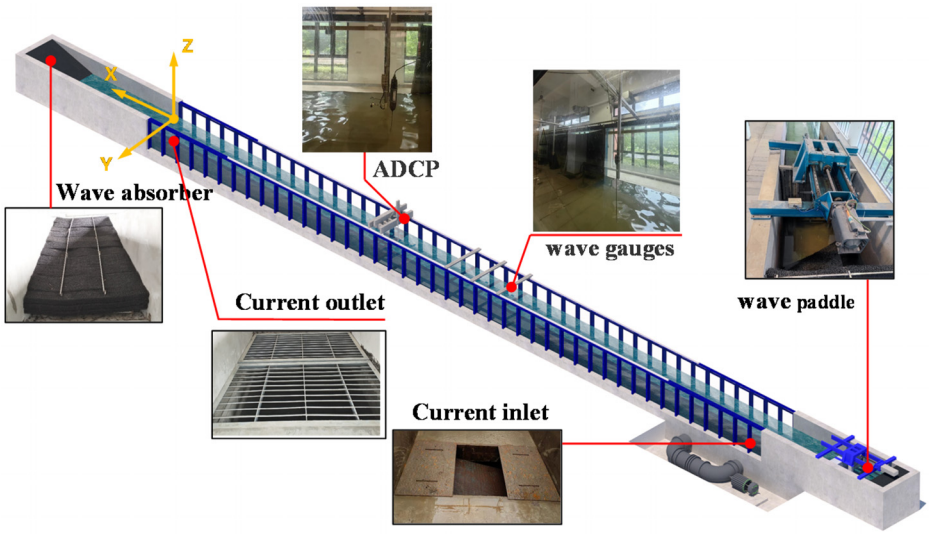

FIG. 2. Wave–current flume and its components.

where a_s is wave amplitude of current-free wave field.

By substituting Eq. (15) into Eq. (16) and combining it with Eq. (10), we can derive the formula for the wave height of the nonlinear wave–current interactions, as shown in the following equation:

$$\frac{a}{a_s} = R\frac{\left\{1+\pi^2\left(\frac{2a_s}{L_s}\right)^2\left[B_s+\frac{3}{8192}\pi^2\left(\frac{2a_s}{L_s}\right)F_s\right]\right\}}{\left\{1+\pi^2\left(\frac{2a}{L}\right)^2\left[B+\frac{3}{8192}\pi^2\left(\frac{2a}{L}\right)F\right]\right\}},$$

$$B = \frac{1}{2}\left(\frac{1}{\tanh kd}\right)^2\left(1+\frac{3}{1+2(\sinh kd)^2}\right)^2+\frac{9}{32}\frac{\cosh 2kd}{(\sinh kd)^6},$$

$$F = 3\left(\frac{1+8(\cosh kd)^8}{(\sinh kd)^6}\right)^2+\frac{1}{2}\frac{\tanh kd\sinh 6kd(11-2\cosh 2kd)^2}{(\sinh kd)^{14}}, \tag{17}$$

where a is wave amplitude of wave–current interaction field.

The wave height is obtained by substituting the obtained wave amplitude and wavelength from Eq. (15) and Eq. (16) into Eq. (17), as shown in the following equation:

$$H = 2a+\frac{2\pi^2a^3}{L^2}\frac{3(1+8\cosh^6 kd)}{16\sinh^6 kd}. \tag{18}$$

III. EXPERIMENTAL SETUP

A. Wave–current flume and instrument layout

The wave–current flume test enables the generation of different wave types by adjusting the wave paddle settings. The flume is 75 m long, 1.8 m wide, and 2.0 m deep. The experimental test section of the flume is fitted with stainless steel slides on both sides of the top of the steel frame, which allows for the installation of aluminum profiles and related instruments to achieve forward and backwards movement of equipment along the x axis. The flume is equipped with a velocity sensor mounting bracket that enables the velocity sensor to move forward and backward (x axis), left and right (y axis), and up and down (z axis) using electric switches, making it easy to feature and facilitate the monitoring of current velocity at target points. The flume was divided into six regions: the wave paddle, wave gauge, acoustic Doppler current profiler (ADCP), wave absorber, current outlet, and current inlet, as shown in Fig. 2.

The current field within the experimental section must be calibrated to ensure compliance with the required current velocity before the wave–current interaction experiment. During the experiment, it is essential to ascertain the time it takes for the current field to stabilize and employ an ADCP to record the time history of the flow field in the experimental tank. The ADCP used in this study has a sampling frequency range of 0–200 Hz, a current velocity measurement range of 0–4 m/s, and an accuracy of 1/1000. The sampling frequency is set to 100 Hz, as shown in Fig. 3.

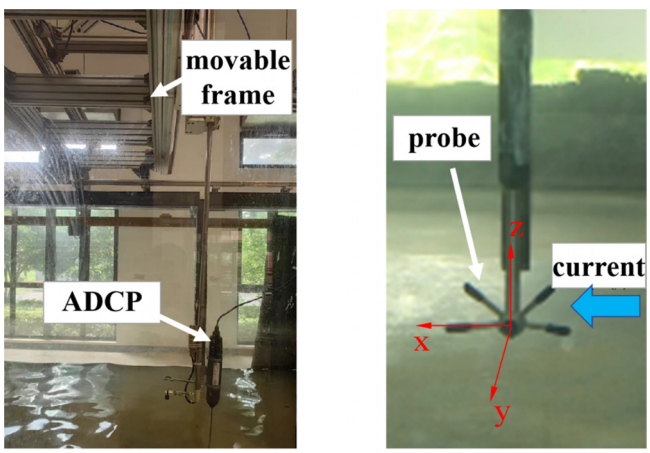

FIG. 3. ADCP layout and acquisition configurations: (a) ADCP layout and (b) ADCP probe and detection direction.

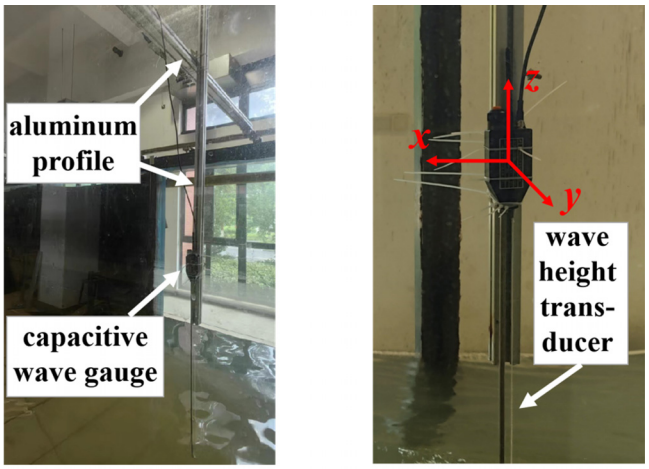

FIG. 4. Wave gauges layout and wave height transducer: (a) Wave gauges layout and (b) wave height transducer and detection direction.

To minimize experimental errors, the wave height transducer is positioned near the still water surface. At least two repeated experiments were conducted for each group to ensure sufficiently low intra-group errors, thereby eliminating the interference of certain unstable factors. The trimmed tail estimation method is employed to further minimize errors in the subsequent processing of wave heights. A wave gauge was used to capture water surface elevations at various locations. The wave gauge has a measurement range of 0–80 cm, a sampling frequency of 100 Hz, and a measurement accuracy of 1/500. The wave gauges are located within the range of 25.5–37.5 m from the start of the flume to ensure full wave development and interaction with the current while preventing wave reflection effects from remaining unabsorbed at the end of the flume, as shown in Fig. 4.

The wave gauges and ADCP are installed in the test section in the middle of the flume, and all the instruments are positioned along the flume's central axis at a distance of 0.9 m from the sidewalls. The initial wave gauge is positioned 22.5 m from the wave generation area, which is 3 m long, as shown in Fig. 5(a). Five wave gauges are arranged linearly to collect waveform variations in the propagation direction, with adjacent gauges spaced 3 m apart, as illustrated in Fig. 5(b). The current profiler is positioned 3 m behind the nearest wave gauge to calibrate the current velocity field. By recording the time it takes for the same wave to pass through different wave gauges in the steady-state field, assuming that the time at which the first wave gauge detects the wave crest is t_1 and the time at which the wave crest arrives at the next wave gauge is t_2, the time difference $\Delta t = t_2 - t_1$ can be obtained. The wavelength L of the steady-state wave field can be determined by combining the distance D between wave gauges and the period T of the waves, using the formula $L = TD/\Delta t$, as shown in Fig. 5(c). The average wavelength of the data collection period can be obtained by summarizing the collected data from different wavebands and instruments and excluding outliers.

B. Experimental conditions

Wave–current interaction experiments covering 33 sets of nonlinear (2–5 order) regular wave types and six different current velocities (0–0.3 m/s) were conducted, covering 164 sets of experimental conditions, including current-free waves, wave-free currents, weak waves and weak currents, and strong waves and weak currents. Experimental investigations of wave–current interactions were conducted to study the influence of water depth and flow velocity on crucial factors such as wave height, wave celerity, and wavelength. The wave heights ranged from 0 to 0.3 m, and experiments were conducted at water depths of 0.4, 0.6, and 0.8 m, with current velocities ranging from 0 to 0.3 m/s, as shown in Table II.

The distribution of the wave periods is shown in Table III, and this condition was not adopted because the breaking phenomenon occurred during the wave-making process without any factors.

C. Verification of the current and wave field

To verify the wave-free current fields, the average current velocity within 60 s is taken as the current velocity at the corresponding water depth after a specific time. The boundary effect of the flume bottom intensifies with the increase in current velocity and decrease in water depth.[30] Due to space limitations, the time history curves of flow velocity at a SWL of 0.4 m, with velocities of 0.05 and 0.2 m/s, respectively, are depicted in Fig. 6. The blue solid line depicts the actual current velocity time-series, the yellow dashed line represents the mean

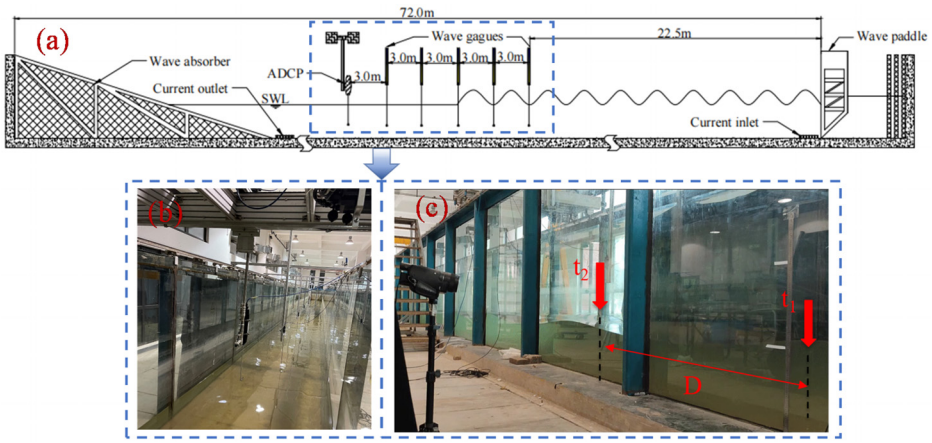

FIG. 5. Instrument layout and wavelength sampling method: (a) wave–current flume, (b) instrument layout, and (c) schematic diagram of wavelength acquisition.

TABLE II. Layout of test conditions. Note: ① represents a water depth of 80 cm, ② represents a water depth of 60 cm, and ③ represents a water depth of 40 cm.

H/m	Arrangement of the test group						
0.30	②	②	②	②	②		
0.25	①②	①②	①②	①②	②		
0.20	①②	①②	①②	①②	②		
0.15	①②③	①②③	①②③	①②③	②③	③	③
0.125	③	③	③	③			
0.10	①②③	①②③	①②③	①②③	②③		
0	①②③	①②③	①②③	①②③	②③		
v/(m/s)	0	0.05	0.1	0.15	0.2	0.25	0.3

TABLE III. Wave period distribution.

H/m	d/m		T/s	
0.30	0.6	···	2	2.5
0.25	0.6,0.8	1.5	2	2.5
0.20	0.6,0.8	1.5	2	2.5
0.15	0.4,0.6,0.8	1.5	2	2.5
0.125	0.4	1.5	2	2.5
0.10	0.4,0.6,0.8	1.5	2	2.5
0	0.4,0.6,0.8	1.5	2	2.5

time-series of filtered velocity, and the red solid line signifies the target current velocity values for various working conditions.

In regions of substantial current velocity, the instability of the current velocity time-series significantly increases. Near the flume bottom, the flow velocity time history shows a decrease relative to the target velocity, but this is confined to a narrow region near the bottom. In this investigation, the thickness of the wave–current boundary layer was taken into account when selecting wave heights, ensuring that the interacted wave–current conditions are within the stable and uniform water current layer. The impact of boundary effects will be further examined in the subsequent analysis of steady-state wave surface times-series, which are illustrated in the Fig. 7(b).

The current velocities at different water depths under different current velocities are plotted in the graph and compared with the current simulated by the numerical simulation software Flow-3D. In the graph, "S" represents the numerical simulation result, while "E" represents the experimental result. "S-0.05," "S-0.1," "S-0.15," and "S-0.2" denote the velocity profiles simulated at four current velocities, while "E-0.05," "E-0.1," "E-0.15," and "E-0.2" represent the velocity profiles of the experiments. The experimental and numerical simulation results are in good agreement, with errors all below 2%. Both methods accurately simulate the current velocities in stable segments, meeting the expected requirements, as shown in Fig. 7(a). To assess the extent of boundary effects, select the maximum wave height under the water depth condition in this experiment, which is 0.15 m. The water surface elevations under various current velocities are shown in the Fig. 7(b).

In Fig. 7, the water surface elevations of current-free wave field are represented by blue dashed lines, while the solid lines represent the water surface elevations of wave–current interaction. It is evident that the water surface elevations do not experience significant deformation across various current velocities, and the impact of boundary effects is effectively controlled within the chosen working conditions.

The free surface height within five cycles of a given period was extracted as the corresponding wavefront equation to calibrate the current-free wave field. The wavefront equations for different wave heights are plotted on the graph using a water depth of 0.6 m and a

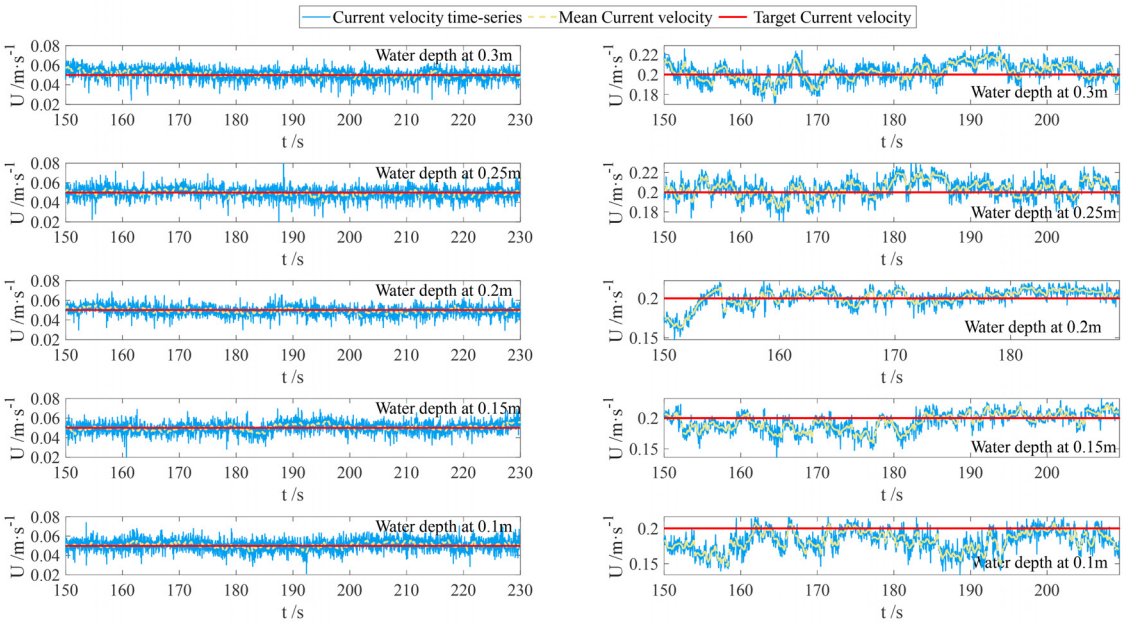

FIG. 6. Time-series of current velocity.

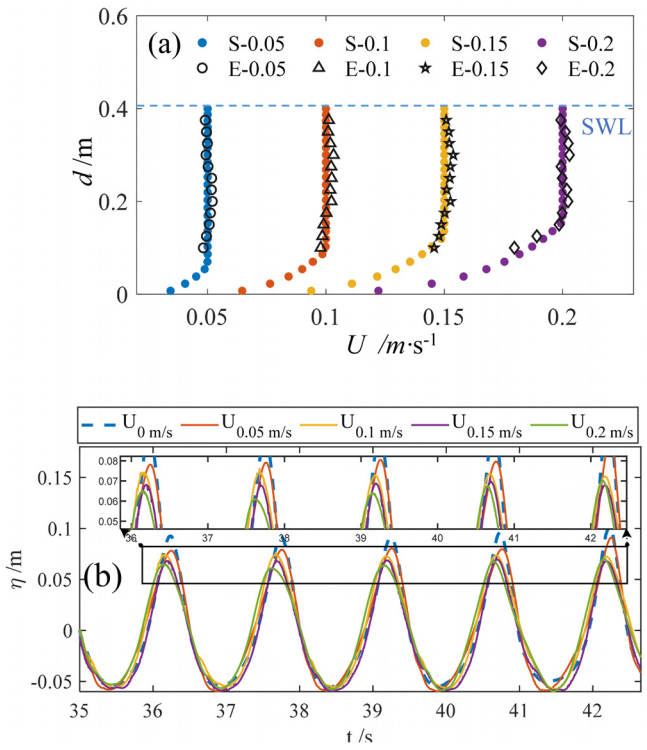

FIG. 7. Wave-free current field verification: (a) current velocity profile, (b) water surface elevations under different currents.

period of 2.5 s as an example. These equations are then compared with the second- and third-order Stokes wave equations.

In Fig. 8, the theoretical wavefront equation results are represented by red dashed lines, while the blue solid lines represent the actual experimental results obtained. The free surface heights for wave heights of 0.1 and 0.15 m fit well with the second-order Stokes wavefront equation. Conversely, the free surface heights of 0.2 and 0.25 m for wave heights agree with the third-order Stokes wavefront equations.

D. Classification of working conditions

The most commonly used method is Le,[31] which uses two dimensionless independent parameters, H/L and d/L, as the vertical and horizontal coordinates, respectively. Various wave theories were selected to approximate the applicable range, as shown in Fig. 9.

The results of the comparisons for different conditions of water depth, period, and wave height are organized and summarized in Table IV and categorized into low-order waves (second-order waves) and high-order waves (third-order waves).

Table IV indicates that the wave height is the most critical factor influencing the wave order. In the case of a current-free wave field, wave heights greater than 0.2 m all satisfy the third-order wave surface equation. In addition, the relative wave height (H/d) is also an essential factor affecting wave nonlinearity. Subsequent research is based on the working conditions of third-order waves in this experiment, aiming to analyze the variation in wave characteristics and the nonlinear effects of third-order waves under the influence of water current.

IV. RESULTS AND DISCUSSION

In the present investigation, the predictions from the proposed model were compared with those from the literature models using two statistical parameters, namely, the mean relative error (MRE) and the determination coefficient (R^2). They are defined as follows:

$$MRE = \frac{1}{m}\sum_{j=1}^{m}\left|\frac{\Phi_{mea,j} - \Phi_{pre,j}}{\Phi_{mea,j}}\right|,$$
$$R^2 = \frac{\left[\sum_{j=1}^{m}\left(\Phi_{mea,j} - \overline{\Phi_{mea}}\right)\left(\Phi_{pre,j} - \overline{\Phi_{pre}}\right)\right]^2}{\sum_{j=1}^{m}\left(\Phi_{mea,j} - \overline{\Phi_{mea}}\right)^2\sum_{j=1}^{m}\left(\Phi_{pre,j} - \overline{\Phi_{pre}}\right)^2}, \quad (19)$$

where m is the total number of measurements; $\Phi_{mea,j}$ and $\Phi_{pre,j}$ are the measured and calculated wavelengths, respectively; and Φ_{mea} and Φ_{pre} are the average values of the measured and calculated wavelengths, respectively.

A. Calculation accuracy of the wavelength

The current-free wave field was verified using the wavelength sampling method, as shown in Fig. 5. Different conditions of the current-free wave field were used to validate the wavelengths, covering various wave heights and water depths, as shown in Table II. Each testing case includes three different periods. The analysis in Fig. 10(a) shows the determination coefficients and average relative errors for pure wavelengths under different changes in wave elements. Furthermore, Fig. 10(b) illustrates the variation trends of the relative errors with wavelength under different theoretical calculations, as shown in Fig. 10.

Both theories exhibit R^2 values higher than 0.99 when calculating wavelengths, indicating their effectiveness in reflecting changing trends. The relative errors of both theories gradually increase as the wavelength increases. However, compared to the traditional linear method, the third-order wave–current theory (TWCIT) proposed in this investigation demonstrates significantly better predictive accuracy, especially in the 2–4 m wavelength range. The proposed third-order wave–current theory in this investigation offers improved predictions of the impact of nonlinear interaction effects caused by shortened periods on wavelengths in the current-free wave field.

Furthermore, further collection and validation of the wavelengths in the steady-state wave–current interaction field were conducted. A comparison was made on the data in the wave region with wavelengths ranging from 2.6 to 3.7 m.

Figure 11 shows that the proposed third-order wave–current theory achieves significantly greater wavelength prediction accuracy than linear theory due to its various wave characteristics and current velocities. Specifically, the R^2 values for the third-order wave–current theory are 0.98 and 0.81, respectively, while the MRE for the third-order wave–current theory is 0.008, which is lower than the MRE of 0.033 obtained from linear theory calculations. Compared to the traditional linear theory, it is worth noting that the proposed theory has been demonstrated to enhance R^2 by 22.5% and reduce the MRE by 75% when calculating the wavelength of a wave–current interaction steady-state field. This paper proposes a computational method to reduce the prediction error of the wavelength in the steady-state wave–current

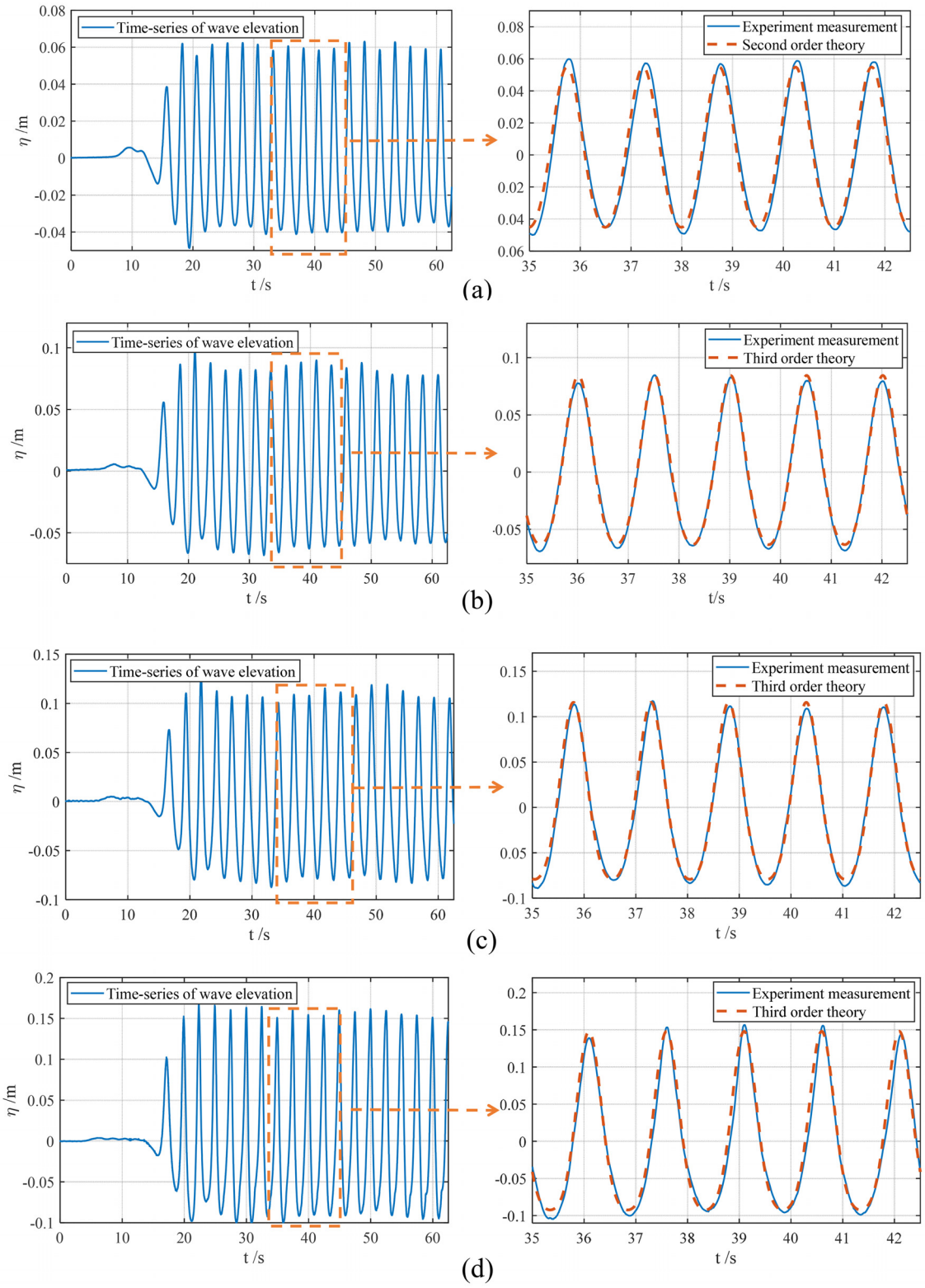

FIG. 8. Comparison of experimental and theoretical water surface elevations under different conditions: (a) *H* is 0.1, (b) *H* is 0.15, (c) *H* is 0.2, and (d) *H* is 0.25 m.

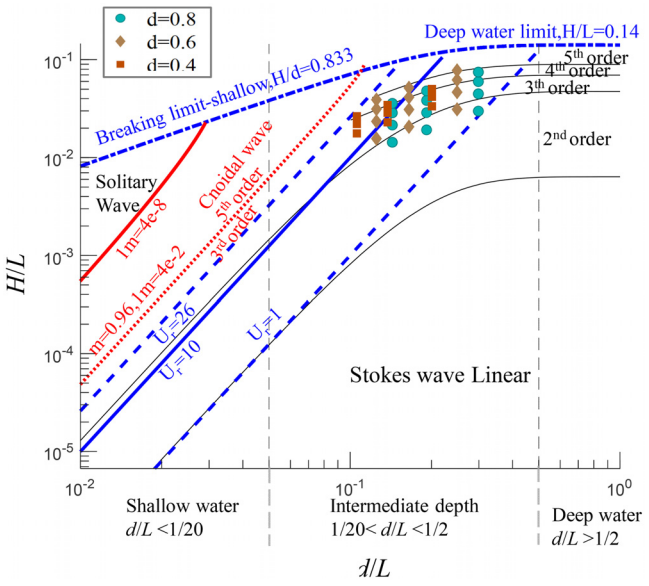

FIG. 9. The wave range in the experimental area.

TABLE IV. Wave-order distribution.

H/m	d/m	T/s	H/L	Stokes wave
0.30	0.6	2.0, 2.5	0.053–0.069	Third order
0.25	0.6,0.8	1.5, 2.0, 2.5	0.039–0.084	Third order
0.20	0.6,0.8	1.5, 2.0, 2.5	0.031–0.067	Third order
0.15	0.4	1.5, 2.0, 2.5	0.032–0.057	Third order
0.15	0.6,0.8	1.5	0.047–0.050	Third order
0.15	0.6,0.8	2.0, 2.5	0.023–0.034	Second order
0.125	0.4	1.5, 2.0, 2.5	0.026–0.048	Third order
0.10	0.4,0.6,0.8	1.5, 2.0, 2.5	0.016–0.038	Second order

field. Linear theory predicts wavelengths that are consistently smaller than the experimental values, indicating insufficient consideration of the effects of nonlinear interactions in wave–current interactions.

B. Verification of wavelength

To further validate the proposed third-order wave–current theory, supplementary material from the literature on the wavelengths of wave–current interactions in steady-state fields were collected due to limitations in experimental conditions. Many researchers have achieved significant results through theoretical analysis or experimental observations.

Li Yucheng's[14] experimental data were compiled to validate the third-order wave–current theory's wavelength theory. The data also included adverse currents not covered in the experiments. The range of periods considered extended from 1.25 to 12 s, while the wave heights ranged from 0.021 to 2.5 m. The water depths ranged from 0.587 to 20.5 m, and the flow velocities ranged from −0.2 to 1 m/s, as shown in Table V.

The analysis results of Table V show that the proposed theory is more sensitive to wave height, enabling a more precise prediction of the nonlinear coupling effects that arise from increases in wave height. Additionally, it maintains good computational accuracy even under reverse flow conditions. It is evident that in the comparison between the two sets of theoretical and experimental data, the theory proposed in this manuscript has high resolution and good fitting performance, meeting the needs of further scientific research.

C. Calculation accuracy of the wave height

This investigation compared the wave height in a steady-state wave–current interaction field using two theories to analyze waves with varying water depths, periods, and heights. The R^2 and MRE increased as the current velocity increased, with six different velocities ranging from 0.05 to 0.3 m considered, as shown in Fig. 12:

The graph shows that for current velocities ranging from 0.05 to 0.1 m/s, there is no significant difference in R^2 between the linear theory and third-order wave–current theory models, as shown in Figs. 12(a) and 12(b). Both have a coefficient higher than 0.99, indicating their effectiveness in reflecting the influence of flow velocity on wave height in the steady-state wave–current interaction field. The proposed third-order wave–current theory can somewhat reduce the relative error caused by neglecting nonlinearity. For current velocities ranging from 0.15 to 0.2 m/s, both theories have R^2 coefficients above 0.98, as shown in Figs. 12(c) and 12(d). The third-order wave–current theory significantly improves the wave height prediction accuracy, with the linear theory achieving the highest MRE of 0.035 at a current velocity of 0.2 m/s. For current velocities ranging from 0.25 to 0.3 m/s, both theories have R^2 coefficients above 0.8, as shown in Fig. 12(e). In the velocity range of 0.05–0.15 m/s, the third-order wave–current theory can reduce the MRE of the linear method by approximately 25%. The third-order wave–current theory can halve the MRE of the linear method when the velocity exceeds 0.15 m/s. This linear theory indicates that as the current velocity increases, the applicability of the traditional linear theory decreases.

To observe changes in the R^2 and MRE of the two theories compared to the experimental data under different wave heights, we considered five different wave heights ranging from 0.1 to 0.3 m, as shown in Fig. 13.

The figure shows that the third-order wave–current theory improves the prediction accuracy compared to traditional linear theory. The interaction effect is satisfactory when the wave height ranges between 0.125 and 0.15 m, with R^2 values consistently above 0.75, as shown in Figs. 13(a) and 13(b). However, at 0.2 m, both the linear theoretical R2 and MRE exhibit a decline in fitting accuracy, as shown in Fig. 13(c). The most significant improvement occurs at a wave height of 0.25 m, where R^2 increases from 0.704 in the linear theory to 0.907, as shown in Fig. 13(d). The comparison of the MREs also favors the third-order wave–current theory over the linear theory, with the most significant improvement observed at a wave height of 0.15 m. When the wave height is in the range of 0.2–0.3 m, the third-order wave–current theory can reduce the MRE by 34%–40% compared to the linear theory, as shown in Figs. 13(c)–13(e). There is a more significant trend of accuracy improvement with increasing wave height. Overall, the third-order wave–current theory reduces the MRE by almost half, better reflecting the influence of the wave height in the current-free wave field on the interacted field wave height.

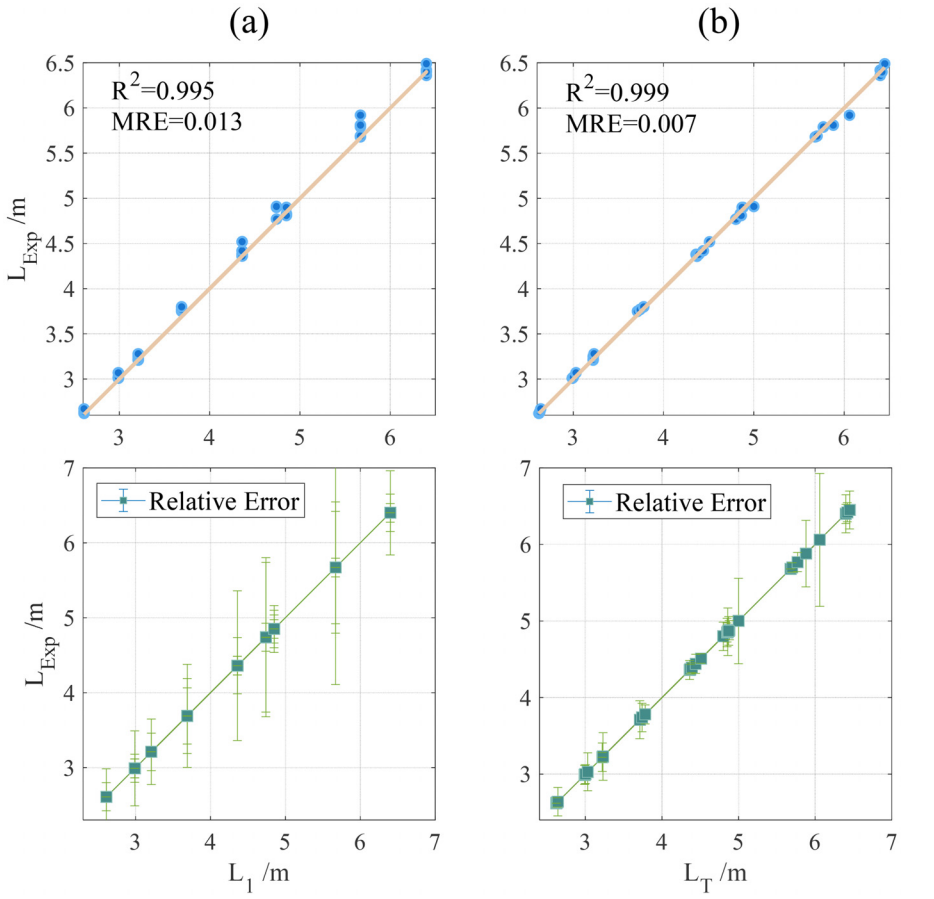

FIG. 10. Data fitting distribution and relative error of the measured and predicted wavelengths for the current-free wave field: (a) traditional linear theory and (b) third-order wave–current theory.

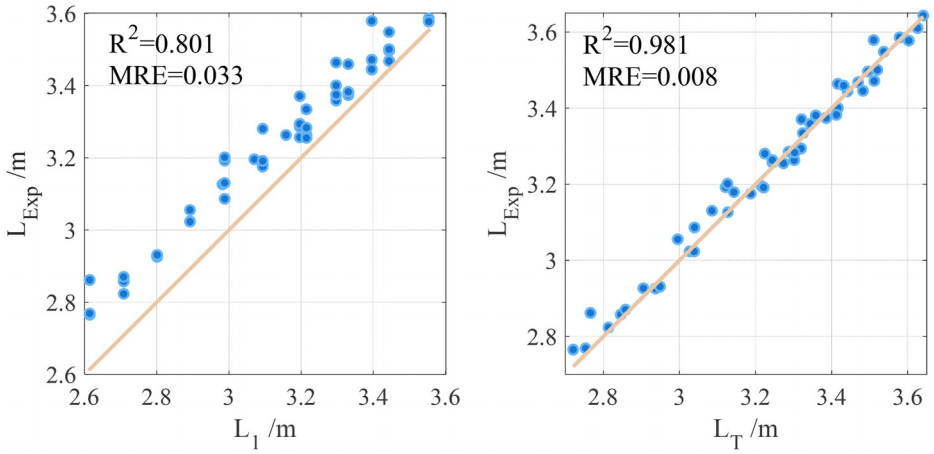

FIG. 11. Theoretical prediction and experimental measurement of the wavelength in high-order regions: (a) linear theory and (b) third-order wave–current theory.

By observing the variations in R^2 and the MRE between the two theories and the experimental data under different periods, three different periods ranging from 1.5 to 2.5 s were considered, as shown in Fig. 14.

It can be observed from the figure that under different period variations, there is no significant difference in R^2 between the linear theory and third-order wave–current theory models, both of which are above 0.99, indicating that they can effectively reflect the influence of the wave periods on the wave–current interaction steady-state field wave height. When the wave period is in the range of 1.5–2.5 s, the third-order wave–current theory can reduce the MRE by 25%–46% compared to the linear theory. The optimal result is observed at a

TABLE V. Working conditions of Li's[14] experimental data.

D (m)	H (m)	T (s)	U (m s^{-1})	L_{Exp} (m)	L_T (m)	L_1 (m)
0.587	0.021	1.25	−0.12	2.05	2.00	1.98
0.57	0.024	1.25	−0.2	1.82	1.81	1.81
30.5	15.2	10	0.9	152.5	152.28	150.7
10	2.5	12	1	130	130.14	126.24

period of 2.5 s. The MRE increases with decreasing wave period, and the proposed third-order wave–current theory can effectively reduce the MRE during different periods.

By observing the changes in the R^2 and MRE of the two theories and experimental data under different water depths, three different water depths ranging from 0.6 to 0.8 m were considered, as shown in Fig. 15.

The graph shows that the R^2 values for linear theory and the third-order wave–current theory increase as the water depth increases. The third-order wave–current theory can reduce the MRE by 31%–44% compared to the linear theory when the water depth is within the 0.4–0.8 m range. The optimal reduction in MRE is observed at a water depth of 0.4 m. The proposed third-order wave–current theory effectively reduces the MRE for different water depths, especially in regions significantly affected by nonlinearity.

The significance of nonlinear effects is determined by three characteristic ratios: wave steepness H/L, relative wave height H/d, and relative water depth d/L. The normalized current U/C in the wave–current coupled field is a crucial coefficient. This investigation collected and organized all MREs for linear theory and third-order wave–current theory methods to analyze the MREs under different characteristic ratios. A value greater than 1 indicates that the third-order wave–current theory proposed in this paper reduces errors under that condition, and a greater value represents a better optimization effect, as shown in Fig. 16.

As shown in the figure above, as U/C increases, the H_1/H_T ratio also increases, mainly when U/C is greater than 0.1. For values below 0.1, the ratio is concentrated between 1 and 2, indicating a significant improvement in accuracy with the proposed third-order wave–current theory. As d/L increases, the data are concentrated in the middle part, and the optimization effect is best in the range of 0.1–0.2. Compared with the experimental results, the linear theory is more applicable in the water depth range of 0.4 m when the wave height decreases to a certain level, as confirmed in Fig. 16(d). The H/d and H/L ratios are similar, with a generally dispersed distribution, but most are greater than 1. With the variation in the characteristic ratios, the third-order

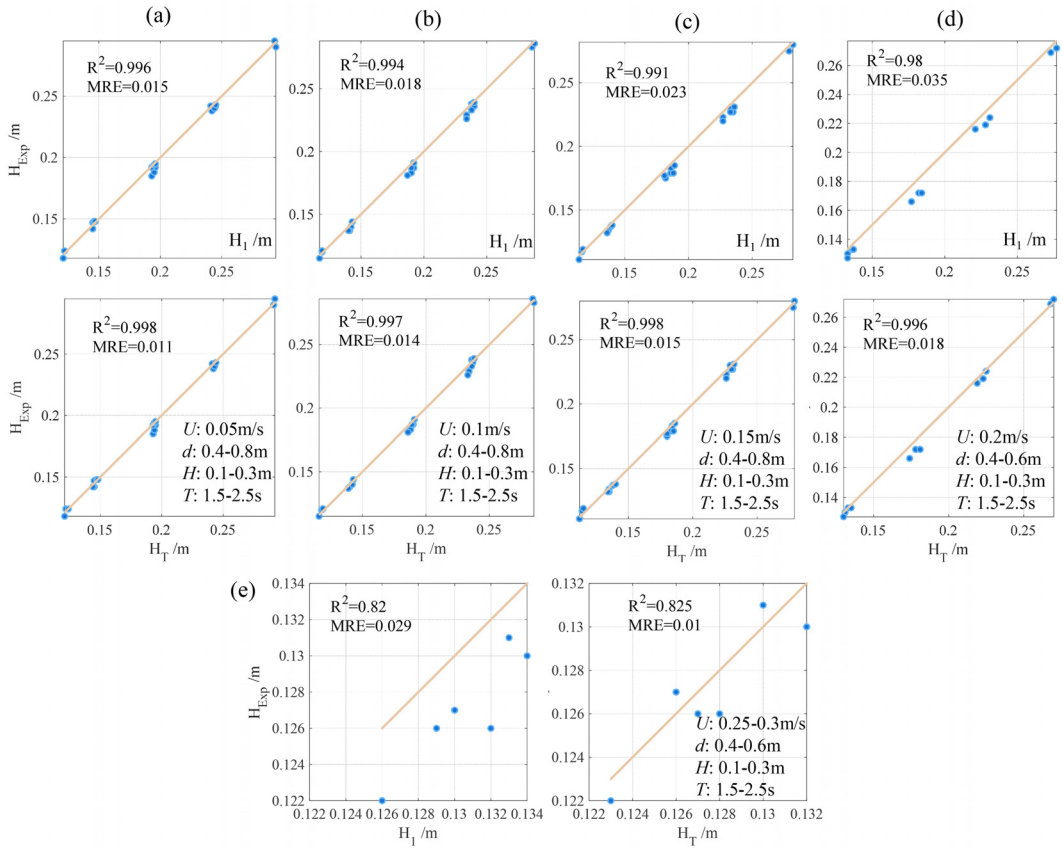

FIG. 12. Theoretical prediction and experimental measurement of the wave height under different current velocities: (a) $U = 0.05$, (b) $U = 0.1$, (c) $U = 0.15$, (d) $U = 0.2$, and (e) $U = 0.25$–0.3.

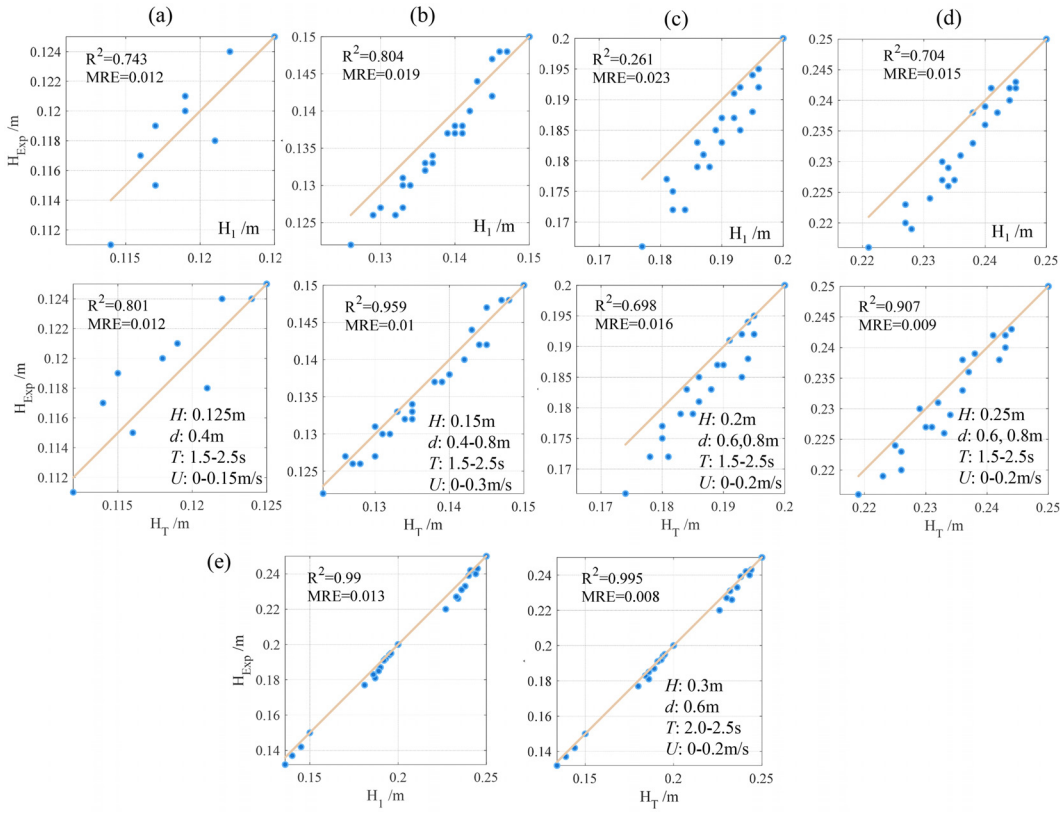

FIG. 13. Theoretical prediction and experimental measurement of wave height under different wave heights: (a) $H = 0.125$, (b) $H = 0.15$, (c) $H = 0.2$, (d) $H = 0.25$, and (e) $H = 0.3$ m.

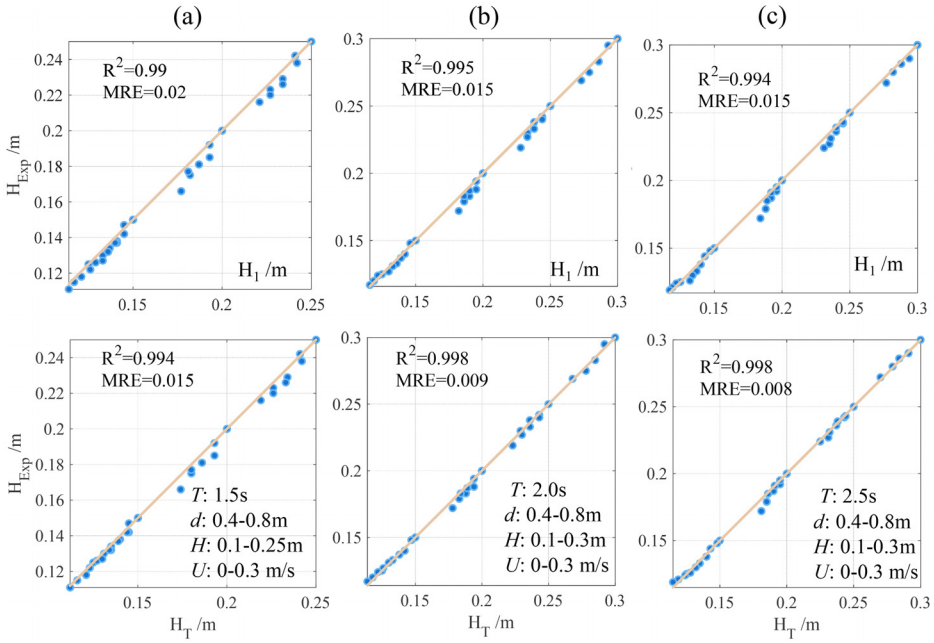

FIG. 14. Theoretical prediction and experimental measurement of the wave height under different wave periods: (a) $T = 1.5$, (b) $T = 2.0$, and (c) $T = 2.5$ s.

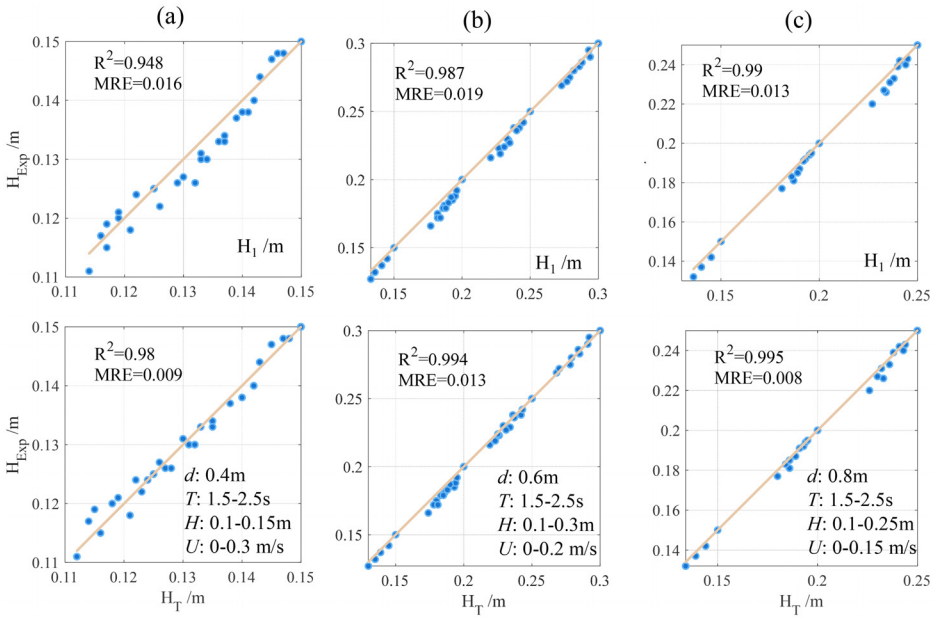

FIG. 15. Theoretical predictions and experimental measurements of wave height at different water depths: (a) $d = 0.4$, (b) $d = 0.6$, and (c) $d = 0.8$ m.

wave–current theory can significantly reduce the computational errors caused by linear methods.

From the analysis results, it is clear that the wave height in the steady-state wave–current field is more evidently affected by H and U than by T and d. This conclusion is consistent with the results of the analyses in Figs. 12 and 16. However, in R^2, the wave height shows more significant variation with d than with T.

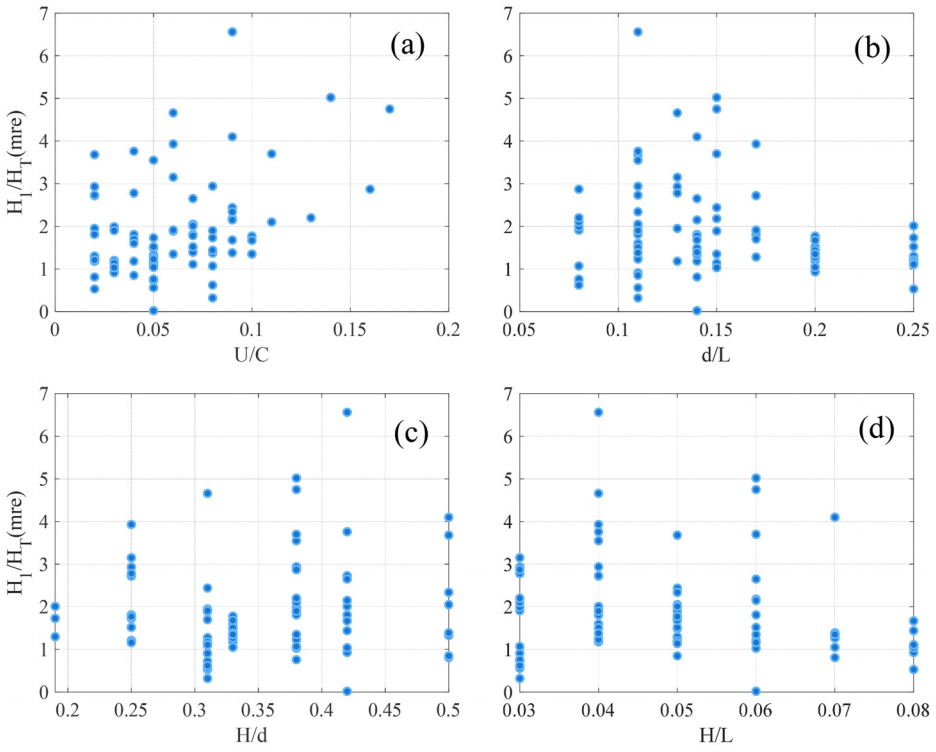

FIG. 16. Variation in two theoretical MRE ratios with varying characteristic ratios: (a) U/C, (b) d/L, (c) H/d, and (d) H/L.

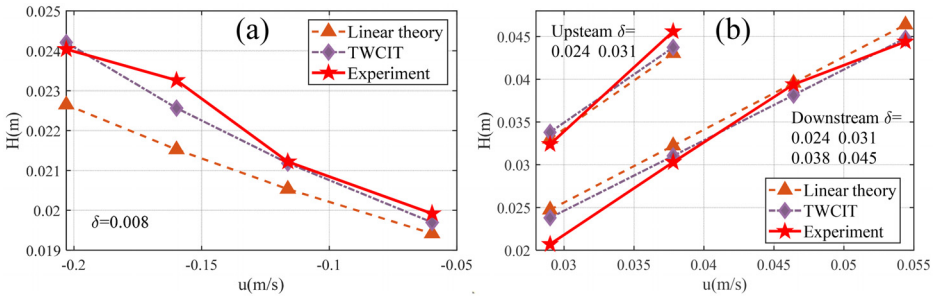

FIG. 17. Comparison of the present numerical results and the experimental data (a) given by Thomas *et al.*[9] and (b) given by Kemp *et al.*[32,33]

D. Verification of wave height

Experimental data on wave–current interactions were collected for Thomas[9] and Kemp and Simons.[32,33] Thomas considered the variation in wave height with current speed, while Kemp considered the influence of wave height and current direction. The factors U (−0.2 m to 0.055 m/s) and H (0.02–0.045) are varied while observing whether the method maintains good simulation results in the case of changes in factors. The third-order wave–current theory is abbreviated as TWCIT, and the results are shown in Fig. 17.

According to Thomas's experimental data, the mathematical formulation of wave height proposed in this manuscript outperforms traditional linear theory at different current speeds, and the theoretical advantage of this manuscript becomes more significant with increasing current speed. By observing Kemp's wave–current interaction experiments with different current directions (upstream and downstream), it can be seen that both theories can fit wave heights well. However, the higher-order wave–current interaction theory proposed in this manuscript can further reduce errors and reflect the wave–current interaction mechanism.

E. Impacts of the key parameters on wave–current interaction

The impact of key factors (U, H, d, and T) on the wave–current interaction was investigated based on third-order wave–current theory and experimental data. Utilizing the third-order wave–current theory to generate a steady-state wave height distribution prediction surface, which incorporates experimental data, enables intuitive observation of

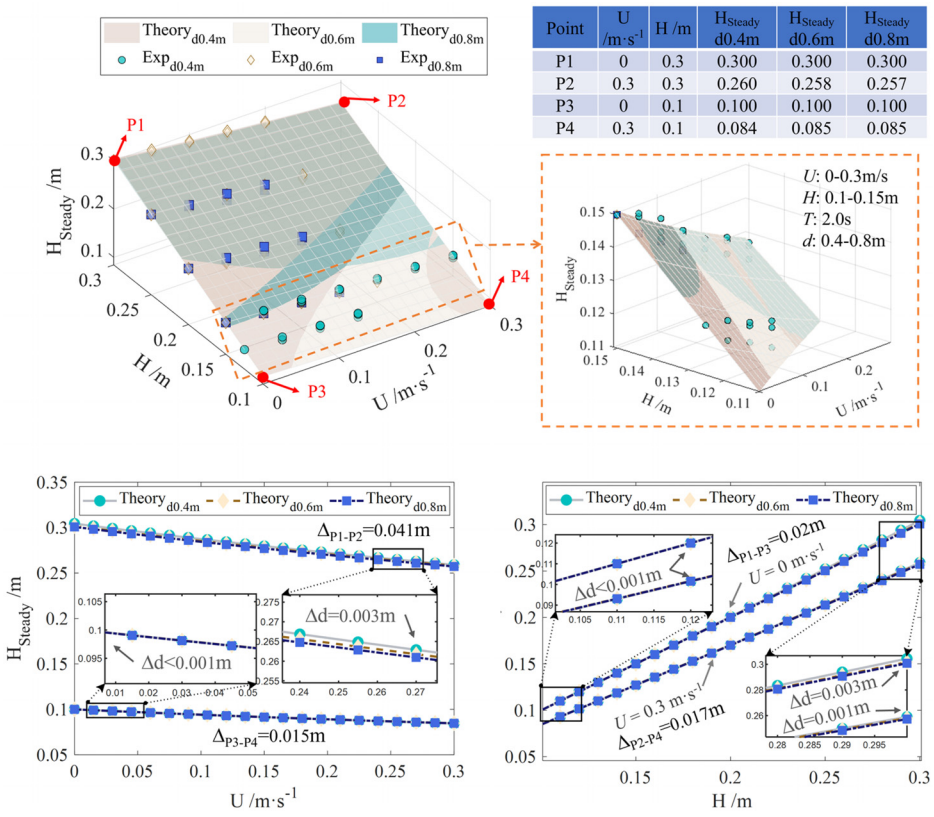

Point	U /m·s^{-1}	H /m	H_{Steady} d0.4m	H_{Steady} d0.6m	H_{Steady} d0.8m
P1	0	0.3	0.300	0.300	0.300
P2	0.3	0.3	0.260	0.258	0.257
P3	0	0.1	0.100	0.100	0.100
P4	0.3	0.1	0.084	0.085	0.085

FIG. 18. Impacts of U, H, and d on wave–current interaction.

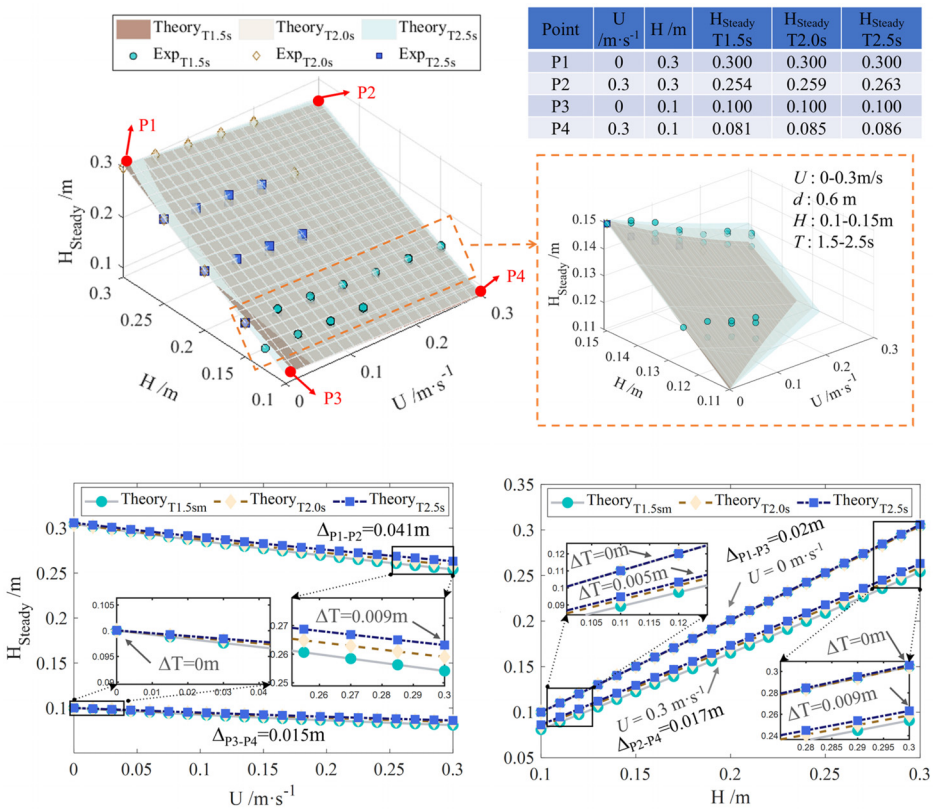

Point	U /m·s^{-1}	H /m	H_{Steady} T1.5s	H_{Steady} T2.0s	H_{Steady} T2.5s
P1	0	0.3	0.300	0.300	0.300
P2	0.3	0.3	0.254	0.259	0.263
P3	0	0.1	0.100	0.100	0.100
P4	0.3	0.1	0.081	0.085	0.086

FIG. 19. Impacts of *U*, *H*, and *T* on the wave–current interaction.

the impact of the current-free wave field wave height (H) and current velocity (U) on the steady-state wave height (H_{Steady}).

Four observation points were established to monitor the H_{Steady} at varying water depths (d) under different U and H, with a wave period (T) of 2.0 s, as illustrated in the upper left of Fig. 18. The detailed data of the observation points are clearly displayed in the table in Fig. 18. A detailed analysis of H at 0.1–0.15 m reveals that the planes calculated by the three theories highly overlap in this area, which is a certain error compared to the experimental data. It can be inferred that water depth is not the main influencing factor in this area, as shown on the upper right side of Fig. 18.

The lower left segment of the Fig. 18 illustrates the trends in H_{Steady} variations for initial H of 0.1 and 0.3 m, under varying U (0–0.3 m/s) and d (0.4, 0.6, and 0.8 m). The two lines in the figure correspond to the P1–P2 and P3–P4 lines, respectively, where ΔP can be calculated from $\Delta P = |H_{Steady}(\text{first point}) - H_{Steady}(\text{last point})|$. Δd represents the absolute value of the maximum difference calculated for different d at the same U and H. Based on the comparative analysis of $\Delta_{P1\text{-}P3}$ and $\Delta_{P3\text{-}P4}$, the impact of U significantly exceeds that of the H, which is consistent with the conclusion obtained by Kumar.[34] It is evident that the higher H, the more significant the impact of U on H_{Steady}. The influence of d on H_{Steady} is considerably less than that of U. At a U of 0.3 m/s, the Δd for a H of 0.3 m is 0.003 m, while the Δd for a H of 0.1 m is 0.001 m. The increase in U reduces the variation in ΔP, as shown in $\Delta_{P1\text{-}P3}$ and $\Delta_{P2\text{-}P4}$, which is consistent with the conclusion obtained by Wolf and Prandle.[35] ΔP. The influence of d is less significant in areas with low H, but as H increase, the influence of different d gradually increases. The ability of the three parameters is ranked in descending order as U, H, and d.

Since the d is not significant on the upper right side of Fig. 18, further studies were conducted on the influence of periods (T: 1.5, 2.0, and 2.5 s) on wave–current interactions under the influence of different factors (U and H). Four observation points were established to investigate the variation of H_{Steady} in varying T, under different U and H, with a d of 0.6 m. Detailed information regarding the observation points can be found in Fig. 19. A detailed analysis of H at 0.1–0.15m reveals significant differences among the three theoretical calculation planes in this area. The derived planes effectively reflect the variation trend of the experimental data under changes in U and H, indicating that the T is the crucial influencing parameter in this area, as shown on the upper right of Fig. 19.

At the same U of 0.3 m/s, the ΔT for an H of 0.3 m is 0.009 m, while the ΔT for an H of 0.1 m is 0.005 m, where ΔT is the absolute value of the maximum difference calculated by different T under the same U and H. The increase in U and H increased the difference in H_{steady} at different T. A comparison of Δd in Fig. 18 and ΔT in Fig. 19 shows that the periodic change has a more significant impact on H_{steady}. The ability of the key parameters to influence the wave–current interaction is ranked in descending order as U, H, T, and d.

V. CONCLUSIONS

This investigation derived a steady-state solution for third-order wave–current theory based on the third-order wave dispersion

relationship and the principle of wave–current energy conservation. The wave–current interaction experiment was set up to cover 164 sets of experimental conditions, including 33 types of periodic waves from the second to the fifth order and six different current velocities. The main conclusions of this paper are summarized as follows:

(1) A total of 164 sets of experimental conditions, including current-free wave, wave-free current, weak wave and weak current, and strong wave and weak current, were used to investigation the effects of water depth and current velocity on crucial characteristics such as wave height, wave celerity, and wavelength in the wave–current interaction field.
(2) In comparison with traditional linear theory, the third-order wave–current theory has been demonstrated to enhance R^2 by 22.5% and reduce the MRE by 75% when calculating the wavelength of a wave–current interaction steady-state field. In the velocity range of 0.05–0.15 m/s, the third-order wave–current theory can reduce the MRE of the linear method by approximately 25%. The third-order wave–current theory can halve the MRE of the linear method when the velocity exceeds 0.15 m/s. When the wave height is in the range of 0.2–0.3 m, the third-order wave–current theory can reduce the MRE by 34%–40% compared to the linear theory. There is a more significant trend of accuracy improvement with increasing wave height. When the wave period is in the range of 1.5–2.5 s, the third-order wave–current theory can reduce the MRE by 25%–46% compared to the linear theory. The optimal result is observed at a period of 2.5 s. The third-order wave–current theory can reduce the MRE by 31%–44% compared to the linear theory when the water depth is within the 0.4–0.8 m range. The optimal reduction in MRE is observed at a water depth of 0.4 m.
(3) Traditional linear methods yield more minor wavelength predictions and more significant wave height predictions in highly nonlinear regions. The wave heights in the steady-state wave–current field are more evidently affected by H and U than by T and d. This conclusion is consistent with the results of Figs. 9–13. However, in R^2, the variation in the wave height is more significant with d than with T. The influence of d is less significant in areas with low H, but as H increase, the influence of different d gradually increases. The increase of U and H increased the difference of H_{steady} at different T. The ability of the key parameters on wave–current interaction is ranked in descending order as U, H, T, and d.

It should be noted that the experiments in this article focused on verifying the variation in wave characteristics after wave–current interactions under the following current conditions, and further preparation experiments are needed to verify adverse current conditions. In addition, this paper's lacks sufficient consideration of the influence of the shear of the velocity profile on wave kinematics and needs further investigation.

ACKNOWLEDGMENTS

This work was supported financially by the National Natural Science Foundation of China (Grant No. 52222804).

AUTHOR DECLARATIONS

Conflict of Interest

The authors have no conflicts to disclose.

Author Contributions

Ming Ni: Conceptualization (equal); Data curation (equal); Formal analysis (equal); Methodology (equal); Software (equal); Writing – original draft (equal). **Kai Wei:** Conceptualization (equal); Formal analysis (equal); Funding acquisition (equal); Investigation (equal); Methodology (equal); Resources (equal); Supervision (equal); Validation (equal); Writing – original draft (equal). **Min Luo:** Methodology (equal); Resources (equal); Supervision (equal). **Jinghua Wang:** Data curation (equal); Formal analysis (equal); Methodology (equal); Supervision (equal); Writing – review & editing (equal).

DATA AVAILABILITY

The data that support the findings of this investigation are available from the corresponding author upon reasonable request.

REFERENCES

[1]J. Zhang, K. Wei, and J. Qin, "Resilience and economic loss assessment of highway bridges in the deep reservoir under near-fault ground motions," J. Bridge Eng. **26**(3), 04021007 (2021).
[2]A. D. Cattrell, M. Srokosz, B. I. Moat *et al.*, "Can rogue waves be predicted using characteristic wave parameters?," J. Geophys. Res.: Oceans **123**(8), 5624–5636, https://doi.org/10.1029/2018JC013958 (2018).
[3]K. Wei, X. Zhong, H. Cai *et al.*, "Dynamic response of a sea-crossing cable-stayed suspension bridge under simultaneous wind and wave loadings induced by a landfall typhoon," Ocean Eng. **293**, 116659 (2024).
[4]I. G. Jonsson, *Wave-Current Interactions, The Sea* (John Wiley & Sons Inc., 1990), Vol. 9, pp. 65–120.
[5]Z. Shen, K. Wei, P. Deng *et al.*, "Probabilistic modeling of horizontal wave-in-deck loads on a square concrete deck," J. Offshore Mech. Arct. Eng. **142**(5), 051702 (2020).
[6]X. Zhang, R. Simons, J. Zheng *et al.*, "A review of the state of research on wave-current interaction in nearshore areas," Ocean Eng. **243**, 110202 (2022).
[7]C. R. Lodahl, B. M. Sumer, and J. Fredsøe, "Turbulent combined oscillatory current and current in a pipe," J. Fluid Mech. **373**, 313–348 (1998).
[8]K. Wei, D. Shang, and X. Zhong, "Integrated approach for estimating extreme hydrodynamic loads on elevated pile cap foundation using environmental contour of simulated typhoon wave, current, and surge conditions," J. Offshore Mech. Arct. Eng. **145**(2), 021702 (2023).
[9]G. P. Thomas, "Wave-current interactions: An experimental and numerical study. Part 1. Linear waves," J. Fluid Mech. **110**, 457–474 (1981).
[10]J. Zhou, J. Liu, and A. Guo, "On wave–current interaction with a horizontal cylinder: Load characteristics and vortex pattern," Phys. Fluids **35**(1), 015111 (2023).
[11]P. J. H. Unna, "Waves and tidal streams," Nature **149**(3773), 219–220 (1942).
[12]M. S. Longuet-Higgins and R. W. Stewart, "Changes in the form of short gravity waves on long waves and tidal currents," J. Fluid Mech. **8**(4), 565–583 (1960).
[13]M. H. Zaman and E. Baddour, "Interaction of waves with non-colinear currents," Ocean Eng. **38**(4), 541–549 (2011).
[14]Y. C. Li, "Changes of wave characteristics under coaction of waves and currents," Mar. Sci. Bull. **3**(3), 1–12 (1984) (in Chinese).
[15]Z. Zou, *Water Wave Theories and Their Applications* (Science Publishing Company, Dalian, 2005), pp. 22–23 (in Chinese).
[16]Y. Y. Chen, H. C. Hsu, and H. H. Hwung, "Particle trajectories beneath wave-current interaction in a two-dimensional field," Nonlinear Processes Geophys. **19**(2), 185–197 (2012).
[17]G. B. Whitham, *Linear and Nonlinear Waves* (John Wiley & Sons, 2011).

[18]B. Zhou, K. Ding, J. Huang *et al.*, "Influence of uniform currents on nonlinear characteristics of double-wave-group focusing," Phys. Fluids **36**(3), 037125 (2024).
[19]R. E. Baddour and S. W. Song, "The rotational flow of finite amplitude periodic water waves on shear currents," Appl. Ocean Res. **20**(3), 163–171 (1998).
[20]A. D. D. Craik and S. Leibovich, "A rational model for Langmuir circulations," J. Fluid Mech. **73**(3), 401–426 (1976).
[21]M. H. Zaman, H. Togashi, and R. E. Baddour, "Deformation of monochromatic water wave trains propagating over a submerged obstacle in the presence of uniform currents," Ocean Eng. **35**(8–9), 823–833 (2008).
[22]H. C. Hsu, Y. Y. Chen, J. R. C. Hsu *et al.*, "Nonlinear water waves on uniform current in Lagrangian coordinates," J. Nonlinear Math. Phys. **16**(1), 47–61 (2021).
[23]A. Constantin, K. Kalimeris, and O. Scherzer, "Approximations of steady periodic water waves in flows with constant vorticity," Nonlinear Anal.: Real World Appl. **25**, 276–306 (2015).
[24]B. Liao, G. Dong, Y. Ma *et al.*, "Modified nonlinear Schrödinger equation for gravity waves with the influence of wind, currents, and dissipation," Phys. Fluids **35**(3), 037103 (2023).
[25]J. Wang, Q. Ma, and S. Yan, "A fully nonlinear numerical method for modeling wave–current interactions," J. Comput. Phys. **369**, 173–190 (2018).
[26]B. B. Zhao, M. J. Li, W. Y. Duan *et al.*, "An effective method for nonlinear wave–current generation and absorption," Coastal Eng. **185**, 104359 (2023).
[27]I. A. Svendsen, *Introduction to Nearshore Hydrodynamics* (World Scientific Publishing Company, 2005).
[28]R. E. Baddour and S. W. Song, "Interaction of higher-order water waves with uniform currents," Ocean Eng. **17**(6), 551–568 (1990).
[29]J. B. Christoffersen and I. G. Jonsson, "A note on wave action conservation in a dissipative current wave motion," Appl. Ocean Res. **2**(4), 179–182 (1980).
[30]J. Yuan and O. S. Madsen, "Experimental and theoretical study of wave–current turbulent boundary layers," J. Fluid Mech. **765**, 480–523 (2015).
[31]B. Le Méhauté, *Explosion Generated Water Waves* (Tetra Tech, Inc., 1969).
[32]P. H. Kemp and R. R. Simons, "The interaction between waves and a turbulent current: Waves propagating with the current," J. Fluid Mech. **116**, 227–250 (1982).
[33]P. H. Kemp and R. R. Simons, "The interaction of waves and a turbulent current: Waves propagating against the current," J. Fluid Mech. **130**, 73–89 (1983).
[34]A. Kumar and M. Hayatdavoodi, "On wave-current interaction in deep and finite water depths," J. Ocean Eng. Mar. Energy **9**(3), 455–475 (2023).
[35]J. Wolf and D. Prandle, "Some observations of wave-current interaction," Coastal Eng. **37**(3–4), 471–485 (1999).